Available online at www.sciencedirect.com
ScienceDirect
Tetrahedron
Tetrahedron 63 (2007) 10161–10168

Novel fluorene/carbazole hybrids with steric bulk as host materials for blue organic electrophosphorescent devices

Wei Li, Juan Qiao,* Lian Duan, Liduo Wang and Yong Qiu*

Key Lab of Organic Optoelectronics and Molecular Engineering of Ministry of Education, Department of Chemistry, Tsinghua University, Beijing 100084, China

Received 31 May 2007; revised 26 July 2007; accepted 28 July 2007
Available online 3 August 2007

Abstract—The problem of self-quenching in organic electrophosphorescence devices has been extensively studied and partially solved by using sterically hindered spacers in phosphorescent dopants. This paper attempts to address this problem by using sterically hindered host materials. Novel fluorene/carbazole hybrids with *tert*-butyl substitutions, namely 9,9-bis[4-(3,6-di-*tert*-butylcarbazol-9-yl)phenyl]fluorene (TBCPF) and 9,9-bis[4-(carbazol-9-yl)phenyl]-2,7-di-*tert*-butylfluorene (CPTBF), have been synthesized and characterized. The compounds exhibit not only high triplet energy (>2.8 eV), but also high glass transition temperature (>160 °C) and thermal stability. The substitution of inert *tert*-butyl groups to the carbazole/fluorene rings of these host molecules has a remarkable effect on the corresponding properties of the host materials, i.e. enhancing the thermal and electrochemical stability, weakening the intermolecular packing, and tuning the solid-state emission. Blue electrophosphorescent devices with enhanced performance were prepared by utilizing the sterically hindered host materials. The devices based on the four *tert*-butyl substituted material TBCPF exhibit unusual tolerance of high dopant concentration up to 20% and marked reduction of efficiency roll-off at higher current, indicating significant suppression of self-quenching effect in organic electrophosphorescent devices by the substitution of steric bulks.

1. Introduction

Organic light-emitting diodes (OLEDs) have been the focus of both academic research and industrial interest because of their potential application in the flat-panel displays and solid lighting resources in the past two decades. In particular, intensive study has been dedicated to the development of transitional metal complex based phosphorescent OLED (PHOLED) owing to its potential to achieve an internal quantum efficiency of 100% by harvesting both singlet and triplet excitons.[1] Typically, the organometallic phosphorescent dyes are doped as the guest into an organic conductive host matrix to reduce the quenching stemmed from the relative long lifetime of triplet excitons. The triplet energy (E_T) of the host material must be higher than that of the guest in order to favor an exothermic energy transfer and to confine the excitons within the emitting guest molecules.[2] Compared to the very efficient green and red devices,[3] blue PHOLEDs are especially challenging since the difficulty in finding suitable host material with an E_T exceeding that of the commonly used blue phosphorescent dyes, such as bis[(4,6-difluorophenyl)pyridinato-*N*,C^2]iridium(III)picolinate (FIrpic, E_T=2.62 eV). A few carbazole derivatives[2b,4] and silicon containing compounds[5] can meet the requirement for high energy, but suffer from thermal and morphological instability as a consequence of their extremely limited π conjugation. In our recent work, we designed and synthesized a fluorene/carbazole hybrid 9,9-bis[4-(9-carbazolyl)phenyl]fluorene (CPF),[6] which we believe to be one of the few triplet host materials that successfully combine both large triplet energy and pronounced morphological stability.[7]

In addition to the efficient energy transfer from the host to the guest and the thermal stability of host materials, triplet–triplet annihilation and self-quenching effect are factors of equal importance to the performance of PHOLEDs. Although high efficiency could be achieved, most phosphorescent devices exhibit significant efficiency roll-off on raising either the doping concentration or the operating current density, which is generally attributed to self-quenching of triplet excitons originated from strong bimolecular interaction of phosphorescent dyes.[1] This problem has been addressed through the introduction of sterically hindered spacers to the phosphorescent dye in a few reports.[8] In this work, we proved that using sterically hindered host material is also an efficient way to overcome the self-quenching effect in blue PHOLEDs. By introducing bulky *tert*-butyl groups on

Keywords: Electrophosphorescence; OLED; Blue emission; Host material; Self-quenching.
* Corresponding authors. Tel.: +86 10 62773109; fax: +86 10 62795137 (J.Q.); e-mail addresses: qjuan@mail.tsinghua.edu.cn; qiuy@mail.tsinghua.edu.cn

0040–4020/$ - see front matter © 2007 Elsevier Ltd. All rights reserved.
doi:10.1016/j.tet.2007.07.104

different segments of our previously reported CPF, which possesses both excellent thermal stability and high triplet energy, we synthesized two novel hosts, namely 9,9-bis-[4-(3,6-di-*tert*-butylcarbazol-9-yl)phenyl]fluorene (TBCPF) and 9,9-bis[4-(carbazol-9-yl)phenyl]-2,7-di-*tert*-butylfluorene (CPTBF). The compounds were prepared efficiently via copper catalyzed C–N coupling reaction. Several reports of oligomeric and polymeric fluorene and carbazole structures with *tert*-butyl groups have also been reported, which otherwise focused on the effect of molecular aggregation and spectral stability.[9] Herein, a systematic comparative study concerning their physical and electroluminescent properties has been carried out and blue PHOLED devices based on the novel hosts have been demonstrated. It was found that the substitution of inert *tert*-butyl groups to the fluorene/carbazole rings of these host molecules not only affects the photophysical properties but also significantly reduces the self-quenching in blue phosphorescent OLED using the hybrids as the host.

2. Results and discussion

2.1. Synthesis and X-ray crystal structure

The chemical structures of the fluorene/carbazole hybrids and the syntheses of TBCPF and CPTBF are depicted in Scheme 1. 9,9-Bis(4-iodophenyl)fluorene (**1**) was prepared from diazotization of 9,9-bis(4-aminophenyl)fluorene followed by treatment with the water solution of potassium iodide. Compound **1** was further converted to 9,9-bis(4-iodophenyl)-2,7-di-*tert*-butylfluorene (**2**) through Friedel–Crafts alkylation. Finally, Ullman C–N coupling reaction of **1** or **2** with corresponding carbazole derivative using copper/18-crown-6 as the catalyst and potassium carbonate as the base afforded the target fluorene/carbazole hybrids in moderate to good yields. The *tert*-butyl substituted compounds are well soluble in common organic solvents such as CH_2Cl_2 and ethyl acetate so that they can be conveniently purified by column chromatography. The compounds were fully characterized by ^{1}H NMR spectroscopy, mass spectroscopy, and elementary analyses.

Single crystals of CPF and TBCPF suitable for X-ray crystallography were obtained via gradient-temperature sublimation. The crystal data are listed in Table 1. The ORTEP presentations with 35% probability ellipsoids and the packing views of the two compounds are revealed in Figures 1 and 2, respectively. In both CPF and TBCPF crystals, the two phenyl-carbazole moieties are orthogonally arranged and connected to the 9-position of the fluorene bridge and each carbazole ring forms a large torsion angle (85.3° for CPF and 71.8° for TBCPF) with the adjacent phenyl ring, indicating non-planarity and rigidity of the molecules. Notice that the two compounds exhibit large different packing motif in spite of their similar 3D molecular configurations. In CPF, each two adjacent molecules stack closely through short edge-to-face C–H$\cdots\pi$ interaction (2.68 Å) between the 3-position of the fluorene ring and the carbazole moiety, whereas in TBCPF, where the carbazole ring is attached with sterically hindered *tert*-butyl groups, such fluorene-to-carbazole contact becomes unfavorable and another face-to-face $\pi\cdots\pi$ interaction (3.59 Å) occurs between two neighboring fluorene moieties. This $\pi\cdots\pi$

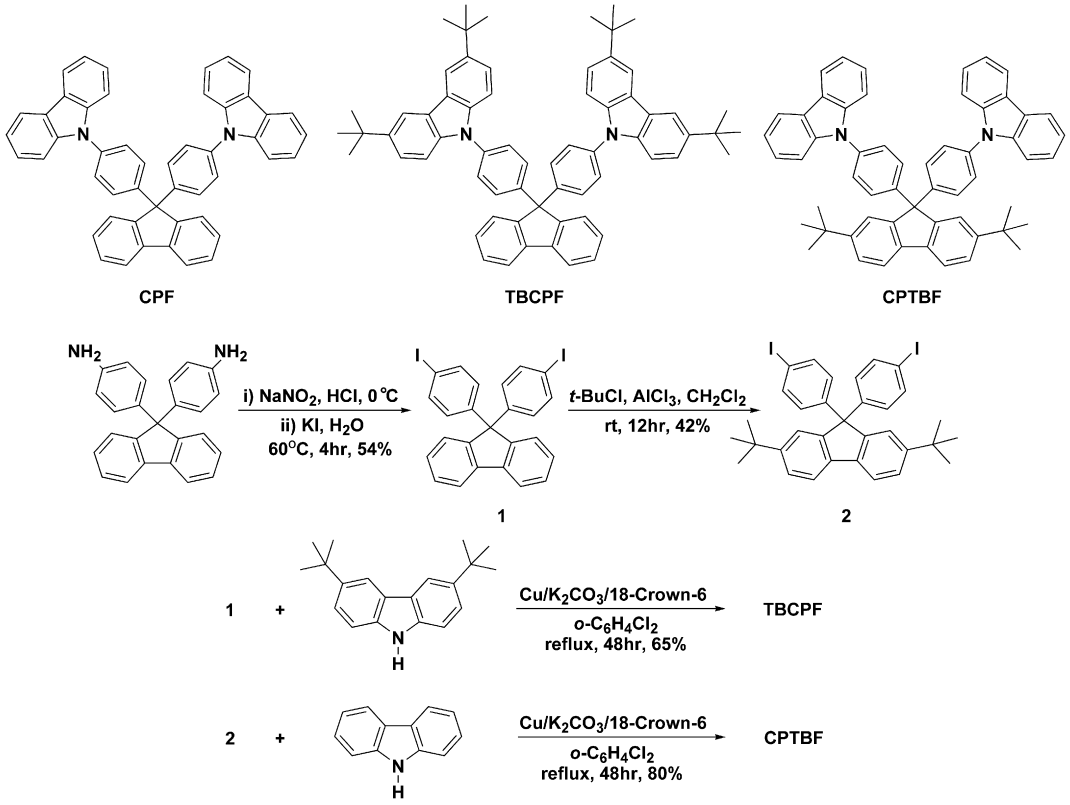

Scheme 1. Chemical structures of the fluorene/carbazole hybrids and synthetic routes to TBCPF and CPTBF.

Table 1. Crystallographic data for CPF and TBCPF

	CPF	TBCPF
Molecular formula	$C_{49}H_{32}N_2$	$C_{65}H_{64}N_2$
Molecular weight	648.77	873.18
Crystal size (mm^3)	0.3×0.3×0.4	0.3×0.2×0.2
Crystal system	Monoclinic	Monoclinic
Space group	*Cc*	*C*2/*c*
a (Å)	22.062(3)	38.594(6)
b (Å)	13.0607(16)	10.9140(18)
c (Å)	15.9859(18)	12.493(2)
α (°)	90	90
β (°)	131.733(2)	98.972(4)
γ (°)	90	90
V ($Å^3$)	3437.5(7)	5197.7(15)
Z	4	4
D_{calcd} (g/cm^3)	1.254	1.116
μ (mm^{-1})	0.072	0.064
$2\theta_{max}$ (°)	55	45
F(000)	1360	1872
Reflections measured	11,516	10,129
R_{int}	0.0285	0.0292
Goodness-of-fit on F^2	1.040	1.040
R_1, wR_2 [$I>2\sigma(I)$][a]	0.0437, 0.0771	0.0794, 0.2128
R_1, wR_2 (all data)[a]	0.0557, 0.0807	0.0946, 0.2267

[a] $R_1=\sum||F_o|-|F_c||/\sum|F_o|$; $wR_2=\left[\sum w(F_o^2-F_c^2)^2/\sum w(F_o^2)^2\right]^{1/2}$.

interaction seems relatively weak since there is a large offset of the fluorene rings involved (see Fig. 2(b)). Moreover, TBCPF possesses a notably lower density (1.116 g/cm^3) than CPF (1.254 g/cm^3). Thus, TBCPF molecules pack more separately from each other and are less inclined to aggregate compared with CPF molecules, which will lead to distinct differences in their physical and optoelectronic properties.

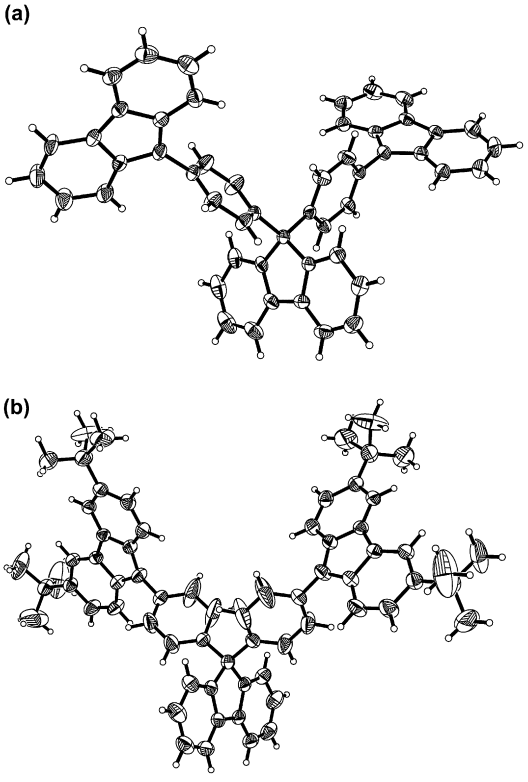

Figure 1. ORTEP drawings of (a) CPF and (b) TBCPF.

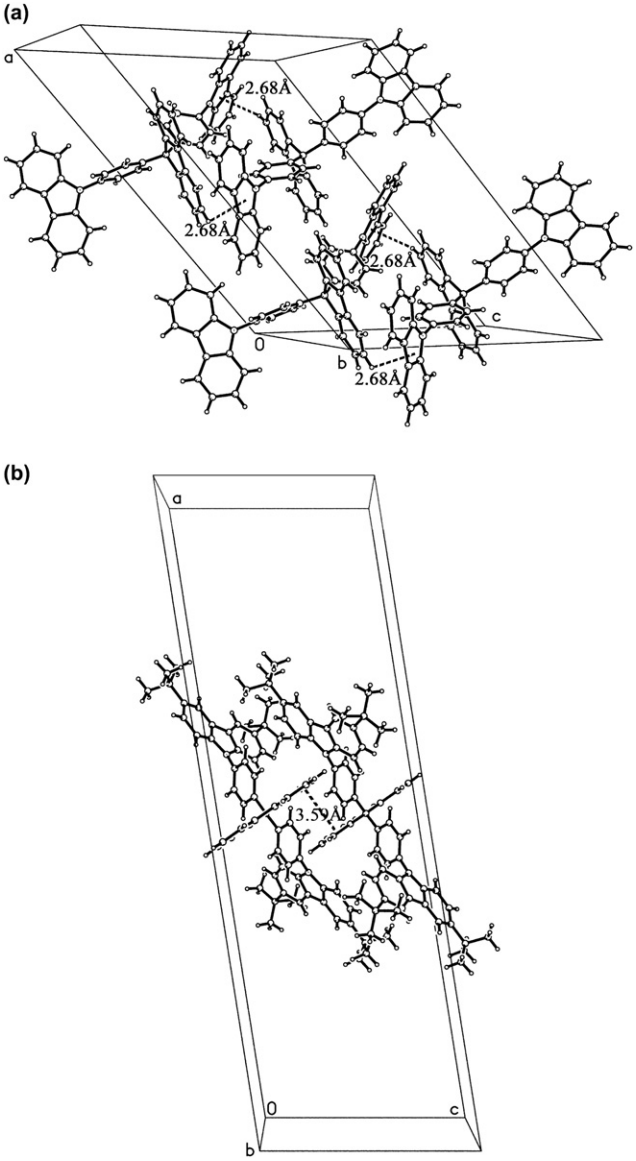

Figure 2. Crystal packing views of (a) CPF, showing the edge-to-face C–H···π contacts and (b) TBCPF, showing the face-to-face π···π interaction.

2.2. Physical properties

Critical data for the physical properties of TBCPF and CPTBF are summarized in Table 2. Data for the non-substituted parent compound CPF are also provided for comparison. The thermal properties of the fluorene/carbazole hybrids were evaluated by thermogravimetric analysis (TGA) and differential scanning calorimeter (DSC). All the compounds form stable glassy states upon rapid cooling from the melts, with glass transition at temperatures higher than 160 °C, followed by crystallization at above 220 °C (Table 2). The thermal decomposition temperatures for TBCPF and CPTBF identified as the peak of the derivative of the weight loss[10] are 540 °C and 511 °C, respectively, which are comparative to the non-substituted CPF. The pronounced thermal stability of the fluorene/carbazole hybrids is ascribed to the hindered and non-planar 3D configuration of the spiro-linkage, which leads to reduction of the tendency to crystallize.[11] It should be noted that

Table 2. Physical properties for the fluorene/carbazole hybrids

Compd	$T_g/T_c/T_d$[a] (°C)	λ_{abs}[b] (nm)	$\lambda_{PL.sol.}$[b] (nm)	$\lambda_{PL.film}$[c] (nm)	$\lambda_{max,phos.}$[d] (nm)	E_T[e] (eV)	E_{ox}[f] (V)	E_{HOMO}/E_{LUMO}[g] (eV)
CPF	165/221/508	293, 328, 342	350, 365	372, 405, 425, 452, 482	431	2.88	1.05, 1.41	5.45/1.91
TBCPF	212/319/540	298, 333, 347	355, 370	357, 374	430	2.88	1.13	5.53/2.05
CPTBF	163/227/511	293, 329, 342	350, 365	351, 367, 401, 423	436	2.84	1.17, 1.50	5.57/2.03

[a] Thermal decomposition temperature (T_d) is defined as the peak of the derivative of the TGA curve.
[b] Recorded in dichloromethane solution.
[c] Recorded in solid film sample.
[d] Phosphorescence peak recorded in 2-methyltetrahydrofuran glasses at 77 K.
[e] Triplet energy estimated from the highest-energy phosphorescence peak.
[f] Onset voltage of the oxidation wave.
[g] HOMO energy level is calculated from the oxidation potentials. LUMO energy level is derived from subtracting the optical band gap from the HOMO energy. The values for CPF are somewhat different with the previous reported values due to different measuring methods.

the introduction of the sterically bulky *tert*-butyl groups does not compromise the morphological stability of the host materials, but even greatly increases both the glass transition temperature and the crystallization temperature in the case of TBCPF (Table 2).

The UV–vis absorption and room temperature photoluminescence (PL) spectra of the fluorene/carbazole hybrids are recorded in dichloromethane solution ($\sim 10^{-5}$ mol/L) and solid state (Table 2). The introduction of steric bulks does not significantly change the photophysical behaviors of the fluorene/carbazole hybrids in dilute solution (Fig. 3). The UV–vis spectra have absorption maxima at around 300, 330, and 340 nm, which are assigned to the π–π^* transitions of the carbazole moiety, whereas the room temperature PL spectra display intense ultraviolet emissions peaked at around 350 and 370 nm. In contrast, the solid-state emissions of the novel hosts with steric bulks differ largely from the parent compound CPF (Fig. 4). The CPF film displays a vibronic feature in the red tail emission with particular emission peaks at 405, 425, 452, and 482 nm, which are not observed in dilute solution, and such emission is independent of the excitation wavelength. We attribute this unusual fine pattern in long-wavelength emission bands in solid state to various degrees of intermolecular aggregation and the excimer formation in the film.[12] CPTBF film also exhibits well-structured PL spectrum, but its low energy emission is less prominent than CPF with only two bands at 401 and 423 nm. However, the TBCPF film exhibits only UV emission with two peaks at 357 and 374 nm, in accordance with the result of its dilute solution, indicating that the emissions from aggregates and excimer are totally suppressed by the bulky *tert*-butyl groups on carbazole rings. This spectral result is consistent with the aforementioned discussion of single crystal structure. Unlike CPF, the introduction of the sterically bulky *tert*-butyl groups on the fluorene/carbazole rings of CPTBF and TBCPF largely reduces intermolecular interaction and sterically separates molecules so that molecular aggregation is suppressed.

The triplet energies of the fluorene/carbazole hybrids were measured from the phosphorescence spectra in 2-methyltetrahydrofuran glasses at 77 K (Fig. 5). The compounds exhibit well-structured phosphorescence bands in the region of 420–520 nm. The triplet energies of TBCPF and CPTBF, which were calculated from the highest-energy phosphorescence peak are 2.84 and 2.88 eV, respectively, which approximate the value of CPF and are high enough for application as the host material for the typical blue triplet emitters.

The electrochemical characteristics of the fluorene/carbazole hybrids were examined by cyclic voltammetry experiments, with ferrocene as internal standard[13] (Table 2). Only oxidative processes were recorded due to the electron-rich nature of carbazole compounds. Both CPF and CPTBF exhibit two distinguished irreversible oxidation waves, indicating that the two carbazole rings are oxidized

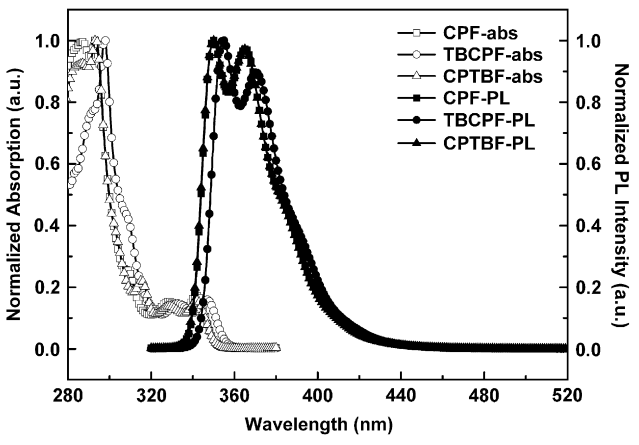

Figure 3. Absorption and room temperature PL spectra (λ_{ex}=300 nm) for the fluorene/carbazole hybrids in dilute CH_2Cl_2 solutions (10^{-5} mol/L).

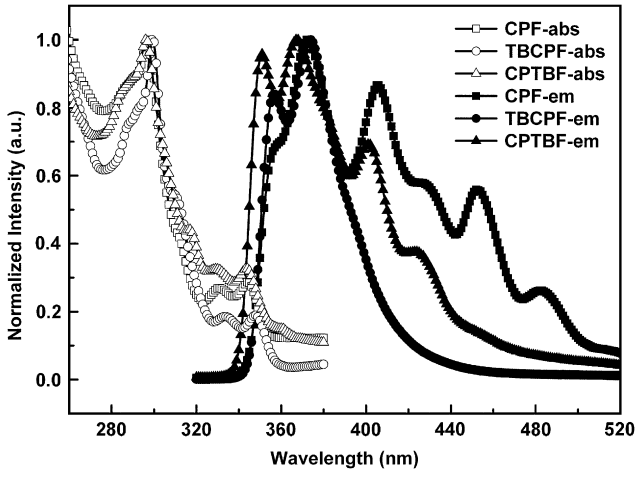

Figure 4. Absorption and PL spectra (λ_{ex}=300 nm) for the fluorene/carbazole hybrids in solid-state films.

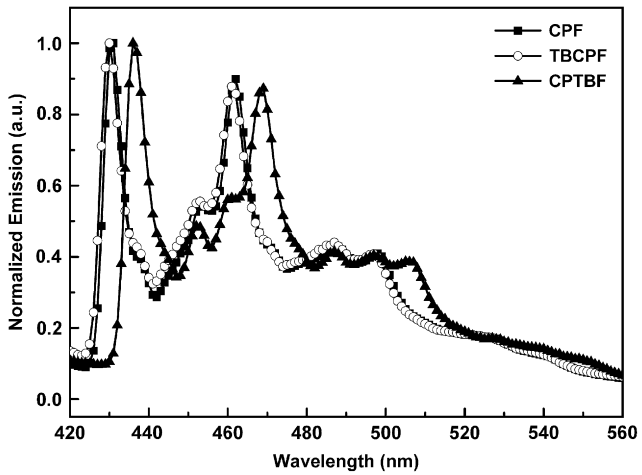

Figure 5. PL spectra (λ_{ex}=300 nm) for the fluorene/carbazole hybrids in 2-methyltetrafuran solutions (10^{-5} mol/L) at 77 K (liquid nitrogen).

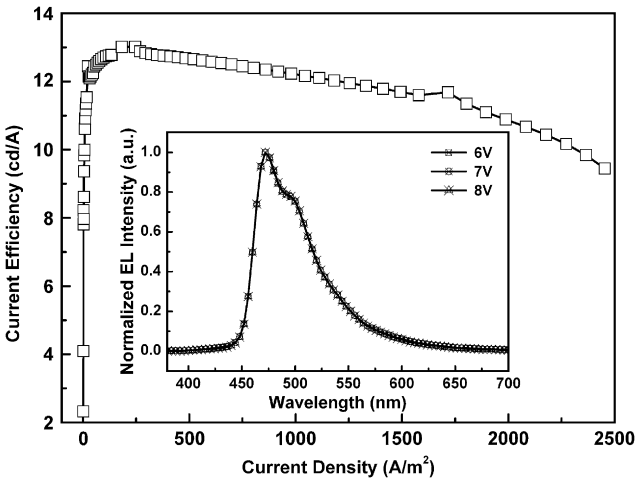

Figure 6. Current efficiency versus current density curve for the device with 20% FIrpic doped in TBCPF. Inset: EL spectrum for the device.

separately. The first oxidative potentials are 1.05 and 1.17 V, respectively. The C–C coupling and polymerization at the electrochemically active 3,6 positions of carbazole rings are responsible for the irreversibility toward oxidation.[7b,14] In contrast, TBCPF, in which the 3,6 positions of carbazole are protected by *tert*-butyl groups, undergoes a reversible oxidation with the onset potential at 1.13 V. The reversibility of the oxidation of TBCPF should enhance the durability of OLED devices since carbazole compounds are responsible for the transportation of positive charge carriers.[14c] The HOMO energy levels of the three compounds were estimated by adding 4.4 to their respective oxidation onset potentials,[15] and the LUMO levels were determined from HOMO levels and optical energy gaps. The results are given in Table 2. Note that the HOMO and LUMO values of CPF are somewhat different from our previously reported values,[6] which were measured using the thin film sample in CH_3CN solution by cyclic voltammetry experiments. The result shows that the introduction of *tert*-butyl groups does not affect the energy levels of the host materials.

2.3. OLED performance

With excellent thermal stability and high triplet state energy, we propose that the fluorene/carbazole hybrids are suitable for use as the host material for blue electrophosphorescence. In particular, TBCPF is expected to have the potential to alleviate the self-quenching of triplet excitons by preventing the aggregation of the phosphorescent dyes. The devices were fabricated based on commercially available blue emitter FIrpic, doped in the fluorene/carbazole hybrids at various mass ratios. The device structure is ITO/NPB(40 nm)/Host: FIrpic(x%, 30 nm)/BPhen(40 nm)/Mg:Ag (x=8, 15, 20 for CPF and 10, 15, 20 for TBCPF and CPTBF), where NPB is *N*,*N*′-biphenyl-*N*,*N*′-(1-naphthyl)-1,1′-biphenyl-4,4′-diamine and was used as the hole-transporting material; BPhen is 4,7-diphenyl-1,10-phenanthroline and was used as the hole blocking and electron-transporting material. Key parameters for the performance of all devices are collected in Table 3. The electroluminescence (EL) spectrum and the efficiency–current density characteristics of the device with 20% FIrpic in TBCPF are plotted in Figure 6 as an example. All the devices only give emissions from FIrpic, indicating complete energy transfer from the host to the dopant. Devices based on CPF, TBCPF and CPTBF exhibit best performance at the doping concentration of 8%, 20%, and 15%, with maximum current efficiency of 11.4, 13.0 and 13.0 cd/A, respectively. Compared with non-substituted CPF, the *tert*-butyl substituted materials TBCPF and CPTBF give improved device performance. As expected, the suppression of concentration quenching by the use of host materials with steric bulk is clearly evident (Table 3). The

Table 3. EL performance of the fluorene/carbazole hybrids as the triplet host

Compound	Doping concentration (%)	Turn-on voltage (V)	L_{max} [a] (cd/m^2)	η_{max} [b] (cd/A)	Efficiency at approx. 100 A/m^2 (cd/A)	Efficiency at approx. 1000 A/m^2 (cd/A)
CPF	8	4.0	21,100 (16.6 V)	11.4	10.3	8.3
	15	5.1	25,800 (15.9 V)	9.5	9.4	7.0
	20	4.9	25,500 (15.7 V)	6.5	5.3	6.4
TBCPF	10	5.2	19,000 (14.6 V)	6.1	6.1	5.4
	15	5.0	25,800 (15.3 V)	11.0	10.9	10.1
	20	4.2	23,300 (12.4 V)	13.0	12.7	12.2
CPTBF	10	4.0	22,600 (14.6 V)	8.6	8.4	7.5
	15	4.3	25,900 (15.3 V)	13.0	12.9	10.4
	20	4.2	21,600 (14.8 V)	6.3	5.6	6.2

[a] Maximal brightness.
[b] Maximal current efficiency.

device based on CPF without *tert*-butyl groups exhibits a sizable decrease in efficiency even at the relatively low doping concentration of 15%. The efficiency of devices based on two *tert*-butyl substituted CPTBF increases dramatically from 8.6 to 13.0 cd/A on raising the doping concentration from 10% to 15%, but still reveals marked quenching on further raising the doping concentration to 20%. However, in the case of the four *tert*-butyl substituted TBCPF, the device efficiency increases with increasing doping concentration even at the very high doping level of 20%, indicating that concentration quenching here is indeed insignificant. Another aspect that reflects the self-quenching effect in PHOLED is the efficiency decrease under high operating current density. We checked the efficiency roll-off at the current density of 1000 A/m^2 for the respective best performing devices of the three compounds (the doping concentrations are 8% for CPF, 20% for TBCPF, and 15% for CPTBF). The efficiency of CPF and CPTBF based devices drops by 27% and 20% from their peak efficiencies, whereas the efficiency roll-off for TBCPF based device is only 6%. Although the maximum efficiency of 13.0 cd/A in our non-optimized devices is somewhat inferior to the reported highest efficiency of blue phosphorescent OLED based on FIrpic,[16] effective suppression of self-quenching in PHOLED by attaching steric bulk to the triplet host material is unambiguously demonstrated here.

3. Conclusions

In summary, we have successfully synthesized fluorene/carbazole hybrids with sterically bulky *tert*-butyl groups for the purpose to explore high performance triplet hosts. Our results suggest that the introduction of *tert*-butyl groups to the triplet host materials can modulate the spectral properties and enhance the device performance without compromising the high thermal stability and triplet energy of the non-substituted parent compound. Blue PHOLED devices using the novel hosts demonstrate that the steric bulks can significantly reduce the self-quenching effect. In particular, the four *tert*-butyl substituted material TBCPF exhibits unusual tolerance of high doping concentration up to 20% and a notable decrease in efficiency roll-off at high current density.

4. Experimental

4.1. General

All chemical reagents were used as received from commercial sources without further purification unless otherwise specified. ^{1}H NMR spectra were recorded on a JOEL JNM-ECA300 NMR spectrometer using tetramethylsilane as an internal standard. EI mass spectrum was collected on a Shimadzu GCMS-QP2010 mass spectrometer. MALDI-TOF mass spectra were collected on a Bruker BIFLEX III mass spectrometer. Elemental analysis data were determined with an Elementar Vario EL CHN elemental analyzer. TGA measurements were carried out on a TA TGA 2050 thermal analyzer. DSC measurements were performed on a TA DSC 2910 modulated instrument at a heating rate of 20 °C/min. Absorption spectra were obtained from an Agilent 8453 UV–vis spectrophotometer. Emission spectra were measured with a HORIBA FluoroMax-3 fluorescence spectrometer. Cyclic voltammetry experiments were conducted on a model CH 600 voltammetric analyzer with a conventional three-electrode configuration, consisting of a platinum plate as the working electrode, a silver wire as the pseudo-reference electrode and a polished platinum wire as the counter electrode. All measurements were carried out at a scan rate of 50 mV/s, with ferrocene as an internal reference. The supporting electrolyte was 0.1 mol/L tetrabutylammonium tetrafluoroborate in CH_2Cl_2 and the solution was bubbled with argon for 15 min prior to the test.

4.2. Synthesis

CPF was prepared by following our previously reported method.[6] 3,6-Di-*tert*-butylcarbazole was prepared according to the literature procedure.[17]

4.2.1. 9,9-Bis(4-iodophenyl)fluorene (1). 9,9-Bis(4-aminophenyl)fluorene (7.0 g, 0.02 mol) was dissolved in a mixture of concentrated hydrochloric acid (12 mL) and water (80 mL), and then cooled to 0 °C. $NaNO_2$ (2.8 g, 0.041 mol, in 15 mL water) was added dropwise to the solution under vigorous stirring. The resulting yellow solution was further stirred for 20 min and subsequently transferred slowly to a solution of KI (12 g, 0.072 mol, in 80 mL water). The reaction mixture was stirred at 60 °C for 4 h. The organic residue was extracted with CH_2Cl_2 (3×50 mL), washed with brine (2×50 mL), dried over Na_2SO_4, and concentrated under reduced pressure to give a yellow solid. The crude product was purified by column chromatography (silica gel, hexane/CH_2Cl_2=10:1) to afford **1** as a white crystalline solid. Yield: 54%. ^{1}H NMR (acetone-d_6): δ 7.91 (d, J=7.5 Hz, 2H), 7.66–7.62 (m, 4H), 7.47–7.39 (m, 4H), 7.35–7.30 (m, 2H), 7.02–6.98 (m, 4H).

4.2.2. 9,9-Bis(4-iodophenyl)-2,7-di-*tert*-butylfluorene (2). Compound **1** (4.0 g, 7 mmol), *tert*-butyl chloride (1.6 mL, 15 mmol), and $FeCl_3$ (0.11 g, 0.7 mmol) were dissolved in CH_2Cl_2 (50 mL). The resulting purple mixture was stirred for 12 h at room temperature, followed by quenching with 10% hydrochloric acid. The organic layer was separated and the aqueous layer was extracted with CH_2Cl_2 (50 mL). The organic layers were combined, washed with brine (100 mL), dried over Na_2SO_4, and concentrated under reduced pressure. The residue was purified by column chromatography (silica gel, hexane) to afford **2** as white crystals. Yield: 42%. ^{1}H NMR (acetone-d_6): δ 7.77 (d, J=7.9 Hz, 2H), 7.66–7.62 (m, 4H), 7.51 (d, J=1.7 Hz, 2H), 7.46 (dd, J=7.9, 1.7 Hz, 2H), 7.05–7.01 (m, 4H), 1.29 (s, 18H). EI-MS: m/z 682 (M^+).

4.2.3. General procedure used for Ullmann condensation. Diiodide (2 mmol) and carbazole derivative (5 mmol) were dissolved in of *o*-dichlorobenzene (40 mL). Copper powder (10 mmol), anhydrous K_2CO_3 (14 mmol), and 18-crown-6 (0.5 mmol) were added to the solution. The reaction mixture was refluxed under argon atmosphere for 48 h and filtered. The filtrate was concentrated under reduced pressure to give a crude product, which was purified by column chromatography (silica gel, petroleum ether/CH_2Cl_2=8:1).

4.2.3.1. 9,9-Bis[4-(3,6-di-*tert*-butyl-9-carbazolyl)phenyl]fluorene (TBCPF). This compound was synthesized according to the general procedure using compound **1** (1.1 g, 2 mmol) and 3,6-di-*tert*-butylcarbazole (1.4 g, 5 mmol). Yield: 65%. ^{1}H NMR ($CDCl_3$): δ 8.12 (d, J=1.4 Hz, 4H), 7.86 (d, J=7.2 Hz, 2H), 7.60 (d, J=7.60 Hz, 2H), 7.48–7.35 (m, 20H), 1.45 (s, 36H). MALDI-TOF MS: *m*/*z* 872.9 (M^+). Anal. Calcd for $C_{65}C_{64}N_2$: C, 89.87; H, 6.49; N, 3.50. Found: C, 89.96; H, 6.36; N, 3.68.

4.2.3.2. 9,9-Bis[4-(9-carbazolyl)phenyl]-2,7-di-*tert*-butylfluorene (CPTBF). This compound was synthesized according to the general procedure using compound **2** (1.4 g, 2 mmol) and carbazole (0.8 g, 5 mmol). Yield: 80%. ^{1}H NMR ($CDCl_3$): δ 8.13 (d, J=7.5 Hz, 4H), 7.74 (d, J=7.9 Hz, 2H), 7.60 (d, J=1.4 Hz, 2H), 7.55–7.36 (m, 18H), 7.30–7.24 (m, 4H), 1.37 (s, 18H). MALDI-TOF MS: *m*/*z* 760.6 (M^+). Anal. Calcd for $C_{57}C_{48}N_2$: C, 89.40; H, 7.39; N, 3.21. Found: C, 89.35; H, 7.37; N, 3.12.

4.3. X-ray crystallography

Single crystal samples of CPF and TBCPF suitable for X-ray crystallography were obtained via gradient-temperature sublimation. The room temperature (294±1 K) single-crystal X-ray experiments were performed on a Bruker SMART APEX CCD diffractometer equipped with graphite monochromatized Mo Kα radiation. Direct phase determination yielded the positions of all non-hydrogen atoms. Hydrogen atoms were generated theoretically and rode on their parent atoms in the final refinement. All non-hydrogen atoms were subjected to anisotropic refinement. Crystallographic data (excluding structure factors) for the structures in this paper have been deposited with the Cambridge Crystallographic Data Centre as supplementary publication nos. CCDC-291117 and CCDC-647969. Copies of the data can be obtained, free of charge, on application to CCDC, 12 Union Road, Cambridge CB2 1EZ, UK (fax: +44-(0)1223-336033 or e-mail: deposit@ccdc.cam.ac.uk).

4.4. Fabrication and characterization of OLEDs

The OLED devices were fabricated on sufficiently cleaned glass substrates precoated with indium tin oxide (ITO). Organic layers were sequentially deposited by thermal evaporation from quartz boats in a high vacuum chamber under the base pressure of around 5×10^{-4} Pa. Then a Mg/Ag (atomic ratio 10:1) layer followed by a Ag cap was evaporated to form the cathode. The luminance–current–voltage (J–V–B) characteristics were determined with a Keithley 4200 semiconductor characterization system. The EL spectra were collected on a Photo Research PR650 spectrophotometer. All the measurements were carried out in air at room temperature without further encapsulation.

Acknowledgements

This work was supported by the National Natural Science Foundation of China (Nos. 50325310 and 50403001) and the National Basic Research Program of China (Grant no. 2006CB806200).

References and notes

1. (a) Baldo, M. A.; O'Brien, D. F.; You, Y.; Shoustikov, A.; Sibley, S.; Thompson, M. E.; Forrest, S. R. *Nature* **1998**, *395*, 151; (b) Baldo, M. A.; Lamansky, S.; Burrows, P. E.; Thompson, M. E.; Forrest, S. R. *Appl. Phys. Lett.* **1999**, *75*, 4.
2. (a) Adachi, C.; Kwong, R. C.; Djurovich, P.; Adamovich, V.; Baldo, M. A.; Thompson, M. E.; Forrest, S. R. *Appl. Phys. Lett.* **2001**, *79*, 2082; (b) Holmes, R. J.; Forrest, S. R.; Tung, Y.-J.; Kwong, R. C.; Brown, J. J.; Garon, S.; Thompson, M. E. *Appl. Phys. Lett.* **2003**, *82*, 2422; (c) Baldo, M. A.; Forrest, S. R. *Phys. Rev. B* **2000**, *62*, 10958.
3. (a) Adachi, C.; Baldo, M. A.; Forrest, S. R.; Thompson, M. E. *J. Appl. Phys.* **2001**, *90*, 5048; (b) Ikai, M.; Tokito, S.; Sakamoto, Y.; Suzuki, T.; Taga, Y. *Appl. Phys. Lett.* **2001**, *79*, 156; (c) Duan, J.-P.; Sun, P.-P.; Cheng, C.-H. *Adv. Mater.* **2002**, *15*, 224; (d) Tung, Y.-L.; Lee, S.-W.; Chi, Y.; Tao, Y.-T.; Chien, C.-H.; Cheng, Y.-M.; Chou, P.-T.; Peng, S.-M.; Liu, C.-S. *J. Mater. Chem.* **2005**, *15*, 460.
4. (a) Adamovich, V.; Brooks, J.; Tamayo, A.; Alexander, A. M.; Djurovich, P.; D'Andrade, B. W.; Adachi, C.; Forrest, S. R.; Thompson, M. E. *New J. Chem.* **2002**, *25*, 1171; (b) Tokito, S.; Iijima, T.; Suzuri, Y.; Kita, H.; Tsuzuki, T.; Sato, F. *Appl. Phys. Lett.* **2003**, *83*, 569; (c) Lei, G. T.; Wang, L. D.; Duan, L.; Wang, J. H.; Qiu, Y. *Synth. Met.* **2004**, *144*, 249.
5. (a) Holmes, R. J.; D'Andrade, B. W.; Forrest, S. R.; Ren, X.; Li, J.; Thompson, M. E. *Appl. Phys. Lett.* **2003**, *83*, 3818; (b) Ren, X. F.; Li, J.; Holmes, R. J.; Djurovich, P. I.; Forrest, S. R.; Thompson, M. E. *Chem. Mater.* **2004**, *16*, 4743.
6. Qiao, J.; Wang, L. D.; Qiu, Y. *Proc. SPIE* **2006**, *6192*, 61920T.
7. (a) Yeh, S.-J.; Wu, M.-F.; Chen, C.-T.; Song, Y.-H.; Chi, Y.; Ho, M.-H.; Hsu, S.-F.; Chen, C. H. *Adv. Mater.* **2005**, *17*, 285; (b) Tsai, M.-H.; Lin, H.-W.; Su, H.-C.; Ke, T.-H.; Wu, C.-C.; Fang, F.-C.; Liao, Y.-L.; Wong, K.-T.; Wu, C.-I. *Adv. Mater.* **2006**, *18*, 1216; (c) Shih, P.-I.; Chiang, C.-L.; Dixit, A. K.; Chen, C.-K.; Yuan, M.-C.; Lee, R.-Y.; Chen, C.-T.; Diau, E. W.-G.; Shu, C.-F. *Org. Lett.* **2006**, *8*, 2799; (d) Tsai, M.-H.; Hong, Y.-H.; Chang, C.-H.; Su, H.-C.; Wu, C.-C.; Matoliukstyte, A.; Simokaitiene, J.; Grigalevicius, S.; Grazulevicius, J. V.; Hsu, C.-P. *Adv. Mater.* **2007**, *19*, 862; (e) Shih, P.-I.; Chien, C.-H.; Chuang, C.-Y.; Shu, C.-F.; Yang, C.-H.; Chen, J.-H.; Chi, Y. *J. Mater. Chem.* **2007**, *17*, 1692.
8. (a) Xie, H. Z.; Liu, M. W.; Wang, O. Y.; Zhang, X. H.; Lee, C. S.; Hung, L. S.; Lee, S. T.; Teng, P. F.; Kwong, H. L.; Zheng, H.; Che, C. M. *Adv. Mater.* **2001**, *13*, 1245; (b) Chew, S.; Lee, C. S.; Lee, S.-T.; He, J.; Li, W.; Pan, J.; Zhang, X.; Kwong, H. *Appl. Phys. Lett.* **2006**, *88*, 093510.
9. (a) Chen, Y.-C.; Huang, G.-S.; Hsiao, C.-C.; Chen, S.-A. *J. Am. Chem. Soc.* **2006**, *128*, 8549; (b) Chen, X.; Tseng, H.-E.; Liao, J.-L.; Chen, S.-A. *J. Phys. Chem. B* **2005**, *109*, 17496; (c) Li, J. Y.; Ziegler, A.; Wegner, G. *Chem.—Eur. J.* **2005**, *11*, 4450.
10. Sapochak, L. S.; Padmaperuma, A.; Washton, N.; Endrino, F.; Schmett, G. T.; Marshall, J.; Fogarty, D.; Burrows, P. E.; Forrest, S. R. *J. Am. Chem. Soc.* **2001**, *123*, 6300.
11. Shen, W.-J.; Dodda, R.; Wu, C.-C.; Wu, F.-I.; Liu, T.-H.; Chen, H.-H.; Chen, C. H.; Shu, C.-F. *Chem. Mater.* **2004**, *16*, 930.
12. Kalonowski, J.; Giro, G.; Cocci, M.; Fattori, V.; Marco, P. D. *Appl. Phys. Lett.* **2000**, *76*, 2352.
13. Gange, R. R.; Koval, C. A.; Lisensky, G. C. *Inorg. Chem.* **1980**, *19*, 2854.

14. (a) Ambrose, J. F.; Nelson, R. F. *J. Electrochem. Soc.* **1968**, *115*, 1159; (b) Ambrose, J. F.; Carpenter, L. L.; Nelson, R. F. *J. Electrochem. Soc.* **1975**, *122*, 876; (c) Brunner, K.; van Dijken, A.; Börner, H.; Bastiaansen, J. J. A. M.; Kiggen, N. M. M.; Langeveld, B. M. W. *J. Am. Chem. Soc.* **2004**, *126*, 6035.
15. De Leeuw, D. M.; Simenon, M. M. J.; Brown, A. R.; Einerhand, R. E. F. *Synth. Met.* **1997**, *87*, 53.
16. Tanaka, T.; Agata, Y.; Takeda, T.; Watanabe, S.; Kido, J. *Jpn. J. Appl. Phys.* **2007**, *46*, L117.
17. Neugebauer, F. A.; Fischer, H. *Chem. Ber.* **1972**, *105*, 2686.